Internal Pipe Area Reconstruction as a Tool for Blockage Detection

Fedi Zouari[1]; Emilia Blåsten[2]; Moez Louati[3]; and Mohamed Salah Ghidaoui, M.ASCE[4]

Abstract: Several pipeline blockage detection methods assume blockages have a regular geometric shape; that is, the blocked section is a pipe of smaller diameter than the original. These methods require a priori knowledge of the number of blockages in the pipeline. Restricting blockages to such special forms also raises identification issues such as nonuniqueness, nonconvergence, and computational inefficiencies. This paper develops a detection method that does not assume regularly shaped blockages and that reconstructs an internal pipe area of unconstrained form. The mathematical and physical bases of the proposed method are described, and a step-by-step solution algorithm is provided. A numerical example of a pipe with irregular blockages is considered to test the performance of the method. It is found that the proposed method accurately identifies multiple blockages of arbitrary shapes and sizes at a relatively low computational cost. The described method is compared with a method for area reconstruction as well as a method for blockage characteristic identification. The proposed method is shown to be more accurate and efficient than the other methods. **DOI: 10.1061/(ASCE)HY.1943-7900.0001602.**

Author keywords: Impulse response; Blockage detection; Transient flow; Area reconstruction.

Introduction

Defects in water supply systems result in significant loss of resources. The presence of blockages increases the energy consumption required to convey the same volume of water, resulting in considerable energy loss and an increase in potential for contamination due to velocity increases and sloughing of material at the blockage location. Unlike some other defects in pipes, blockages are difficult to detect as there are no external visible indicators, nor do they induce detectable sounds (as leakages do) under steady-state flow conditions. However, it is known that blockages cause a detectable change in transient waveforms that can be used for blockage detection (Wang et al. 2005; Mohapatra et al. 2006; Sattar et al. 2008; Duan et al. 2012b; Meniconi et al. 2013; Scola et al. 2017; Louati et al. 2017; Zouari et al. 2017).

There are two primary approaches that can be used to detect blockages using hydraulic transient probing waves and waveform information. The first approach assumes a blocked pipe to be equivalent to a series of circular pipes of different lengths and diameters [Fig. 1(a)] (Wang et al. 2005; Mohapatra et al. 2006; Duan et al. 2012b; Meniconi et al. 2013; Scola et al. 2017; Louati et al. 2017; Zouari et al. 2017). Blockages of this special form are called regular blockages. This approach is referred to as regular blockage detection. The second approach considers more realistic blockages, which may have a continuously varying cross-sectional area $A(x)$ [Fig. 1(b)] (Gong et al. 2014; Massari et al. 2015). Blockages of this general form are called irregular blockages. This approach is referred to as area reconstruction.

In urban water supply systems (UWSSs), regular blockage detection is more commonly used. This is because, in practice, blockage location and size (i.e., diameter) are the most critical characteristics. Moreover, regular blockage detection is considered simpler than area reconstruction as the number of unknown variables is limited to three variables per blockage, while in area reconstruction, $A(x)$ is to be determined. Last but not least, an analytical solution of the transient response of pipes with regular blockages [Fig. 1(a)] can be easily obtained from transfer matrix (Eisner 1967; El-Raheb and Wagner 1982; Bonder 1983; Duan et al. 2012b; Chaudhry 2014). However, there are several disadvantages in using regular blockage: (1) the analytical solution is formulated only for special types of blockages, and therefore irregular-shaped blockages [Fig. 1(b)] cannot be easily accounted for; (2) the total number of blockages in the system needs to be assumed (known) a priori; (3) the number of unknown variables, and therefore the computational complexity, increases rapidly when multiple blockages of irregular shape are considered; and (4) the solution (identification) is not unique unless nontrivial geometrical constraints are imposed (Bonder 1983).

The area reconstruction approach is not commonly used in UWSSs, but has been used in other fields of acoustics. For instance, to teach deaf persons how to speak, researchers developed methods for vocal tract shape reconstruction using acoustic measurements (Schroeder 1967; Heinz 1967; Gopinath and Sondhi 1970; Sondhi and Gopinath 1971; Sondhi 1979; Sondhi and Resnick 1983). Furthermore, Bruckstein and Kailath (1987) showed that methods developed for other applications (physics and mathematics, geophysics, network theory, etc.) can be applied to vocal tract area reconstruction and vice versa. In theory, many area reconstruction

[1]Ph.D. Candidate, Dept. of Civil and Environmental Engineering, Hong Kong Univ. of Science and Technology, Kowloon, Hong Kong (corresponding author). Email: zouari.fedi@gmail.com; fzouari@connect.ust.hk

[2]Postdoctoral Fellow, Jockey Club Institute for Advanced Study, Hong Kong Univ. of Science and Technology, Kowloon, Hong Kong. Email: emilia.blasten@iki.fi

[3]Research Assistant Professor, Dept. of Civil and Environmental Engineering, Hong Kong Univ. of Science and Technology, Kowloon, Hong Kong. Email: mzlouati@gmail.com

[4]Chair Professor and Chinese Estates Professor of Engineering, Dept. of Civil and Environmental Engineering, Hong Kong Univ. of Science and Technology, Kowloon, Hong Kong. Email: ghidaoui@ust.hk

Note. This manuscript was submitted on January 10, 2018; approved on November 21, 2018; published online on March 30, 2019. Discussion period open until August 30, 2019; separate discussions must be submitted for individual papers. This paper is part of the ***Journal of Hydraulic Engineering***, © ASCE, ISSN 0733-9429.

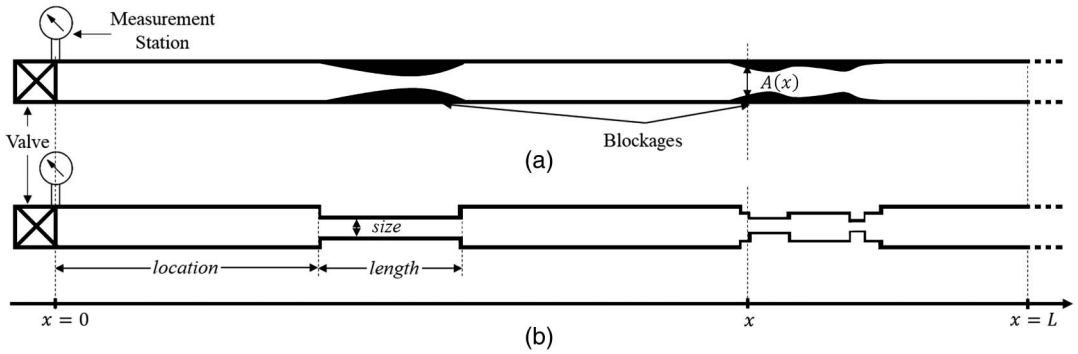

Fig. 1. Blocked pipe: (a) arbitrary blockage shape (irregular blockages); and (b) simplified blockage shape (regular blockages).

methods can be applied to water supply systems. However, choosing a suitable one depends on the type of measurements available. For example, if an area reconstruction method requires an accurate measurement of a transient flow rate, it cannot be easily applied in UWSSs because the transient flow rate cannot be accurately measured in water pipes with existing flow measurement technologies.

In this paper, an area reconstruction method originally proposed by Sondhi and Gopinath (1971) for vocal tract shape reconstruction is adopted for blockage detection in water supply systems. As the area reconstruction approach is not well known to water system engineers, a comprehensive illustration and detailed algorithm of the method is provided in the section "Proposed Blockage Detection Method." A numerical test case of irregularly shaped blockages with and without friction is considered for illustration and discussed in the section "Numerical Results." A comparison of the proposed area reconstruction method and two other blockage detection methods is carried out in the section "Comparison with Other Methods" to illustrate advantages of the proposed method.

Proposed Blockage Detection Method

Theoretical Background

Consider a pipe with a cross-sectional area $A(x)$ and a wave speed $a(x)$, bounded by a valve (or other transient-generating device) at $x = 0$ as shown in Fig. 1(a). The one-dimensional water hammer equations are assumed to govern the pipeline flow (Wylie et al. 1993; Ghidaoui et al. 2005; Chaudhry 2014) [Eqs. (8) and (9)]. For simplicity, flow is assumed frictionless and initially stagnant; that is, the flow rate $Q(x, t)$ is equal to zero and the pressure head $H(x, t)$ is constant and equal to H_0 for $t < 0$. In a later section, friction and initially nonstagnant flow [$Q(x, t) \neq 0$] are considered.

At $t = 0$, a transient flow is generated by a flow impulse at $x = 0$ [i.e., $Q(0, t) = \forall_0 \delta(t)$, where $\forall_0$ is the volume injected; and $\delta(t)$ is the Dirac delta function]. The resulting variation in pressure head, normalized by the initial pulse, at $x = 0$, $\Gamma(t) = [H(0, t) - H_0]/\forall_0$, is therefore called the impulse response function (IRF) and is measured for a time of duration $2L/a_0$ seconds (a_0 being the mean wave speed in the pipe). With this short time measurement, the internal pipe area $A(x)$ is reconstructed for $x \in [0, L]$.

Because of the linearity and time invariance of the water hammer equations, the IRF can be used to determine any pressure head response from any given type of input (Chen 1998). Equivalently, the IRF can be used to determine a special input $Q_{1,\tau}(0, t)$ that induces a constant pressure head, $H(x, \tau) = H_0 + h_0$, at time $t = \tau$. Such an input $Q_{1,\tau}(0, t)$ can be shown to satisfy the following equation (See Appendix I for details):

$$Q_{1,\tau}(0,t) + \frac{1}{2}\int_0^{2\tau} Q_{1,\tau}(0,s) r_m(|t-s|) ds = \frac{gA(0)}{a(0)} h_0 \qquad (1)$$

where $r_m(t)$ = reflected impulse response (RIR) and relates to the measured pressure head by $\Gamma(t) = [H(0, t) - H_0]/\forall_0 = [a(0)/gA(0)][\delta(t) + r_m(t)]$. In this paper, measurement is performed by numerical simulation. The design of an input that satisfies a prescribed response is generally called valve stroking in the context of water hammer (Wylie et al. 1993). It is the crux of the modern boundary control method (Belishev 1997) and the classical work on Gel'fand-Levitan-Krein's equations (Bruckstein and Kailath 1987).

It is shown in Eqs. (14) and (27) in Appendix I that the special input $Q_{1,\tau}(0, t)$ can be used to determine the internal pipe area $A(x)$:

$$A[x(\tau)] = \frac{a[x(\tau)]}{gh_0} \frac{d}{d\tau} \int_0^{\tau} Q_{1,\tau}(0,t) dt \qquad (2)$$

where $x(\tau)$ = location at which a wave traveling from $x = 0$ arrives after time τ [e.g., for a constant wave speed $a(x) = a_0$, $x(\tau) = a_0\tau$]. Eq. (2) shows that, if the wave speed $a(x)$ and $Q_{1,\tau}(0, t)$ for $t \in [0, \tau]$ are known, then the area $A(x(\tau))$ can be obtained. Other cases where the wave speed $a(x)$ is not known are discussed in the last paragraph of Appendix I. For simplicity, the wave speed is considered constant with $a(x) = a(0) = a_0$ elsewhere in this paper.

The impulse response function from $t = 0$ to $t = 2L/a_0$ is used to solve Eq. (1) for the function $Q_{1,\tau}$. Then Eq. (2) is used to solve for the area $A(x)$. It should be noted that the information for the right-side boundary condition at $x > L$ is not used during the area reconstruction because the measurement period used is only $2L/a_0$ s long. This contrasts with many methods in the literature, especially frequency domain methods (e.g., Schroeder 1967; Heinz 1967; Gopinath and Sondhi 1970; Qunli and Fricke 1990; De Salis and Oldham 1999, 2001; Duan et al. 2012b; Scola et al. 2017; Zouari et al. 2017; Louati et al. 2017), and constitutes a major advantage for the proposed method. It is for this reason that the right boundary is not shown in Fig. 1. In the next section, implementation of the proposed area reconstruction method for practical scenarios (numerical data) is further discussed.

Implementation of the Algorithm

The numerical algorithm used to apply the method of the previous section is discussed here.

Step 1
Send an impulse $Q(0,t) = \forall_0 \delta(t)$ and measure the pressure head response denoted by $H(0,t)$ for $0 \le t < 2L/a_0$, where L is the distance up to which the pipe is examined. Given the pressure head measurement, calculate the IRF $\Gamma(t) = [H(0,t) - H_0)]/\forall_0$, then extract the RIR $r_m(t)$ such as $[gA(0)/a_0] * \delta(t)$. An example of the application of this step is shown in Appendix II.

Step 2
Use $r_m(t)$ obtained from Step 1 to deduce the functions $Q_{1,\tau}(0,t)$ for different values of τ. For any value of τ, Eq. (1) is solved numerically. To do this, let $\mathbf{q}_{1,\tau}$ be the vector representing $Q_{1,\tau}(0,t)$ in the interval $t \in [0, 2\tau]$:

$$\mathbf{q}_{1,\tau} = \{Q_{1,\tau}(0,0), Q_{1,\tau}(0,\Delta t), \ldots, Q_{1,\tau}[0,(2N-1)\Delta t]\}^T \quad (3)$$

where superscript T = transpose operator; Δt = discrete time step; and $N\Delta t = \tau$. The integral in Eq. (1) is computed by a rectangular approximation. As a result, Eq. (1) is written as a system of linear equations (Appendix III)

$$\mathbf{H}\mathbf{q}_{1,\tau} = \frac{gA(0)}{a_0}\mathbf{h}_0 \quad (4)$$

where $\mathbf{H} = 2N \times 2N$ matrix such that $\mathbf{H}(i,j) = \delta_{i,j} + \Delta t \times r_m(|i-j|\Delta t)/2$ in which $\delta_{i,j}$ = Kronecker delta function and $\mathbf{h}_0 = 1 \times 2N$ vector with all elements equal to h_0. The vector $\mathbf{q}_{1,\tau}$ is obtained by inverting the matrix $\mathbf{H}$. The matrix $\mathbf{H}$ is a Toeplitz matrix; hence, the vector $\mathbf{q}_{1,\tau}$ can be alternatively solved for by faster algorithms such as the Levinson algorithm or least-squares fitting. An example of the application of this step is shown in Appendix II.

Step 3
Compute the value of the integral of $Q_{1,\tau}$ for different values of τ. Let $\forall(\tau)$ denote the value of the integral of $Q_{1,\tau}$ in the right-hand side of Eq. (2). The value of $\forall(\tau)$ at $\tau = i\Delta t$, $i \in \{0, 1, \ldots, M\}$ with $M\Delta t = L/a_0$, is approximated numerically as follows:

$$\forall(i\Delta t) = \frac{1}{2}\sum_{j=0}^{j=2i} Q_{1,i\Delta t}(0, j\Delta t)\Delta t \quad (5)$$

Here, the integral of $Q_{1,\tau}(0,t)$ is instead computed from $t = 0$ to $t = 2\tau$ and then divided by 2, because $Q_{1,\tau}(0,t)$ is symmetric with respect to τ. This gives more stable numerical results. An example of the application of this step is shown in Appendix II.

Step 4
Compute the estimated area $A(x)$. The area $A(x)$ can be calculated at different locations $x(i\Delta t) = ia_0\Delta t = i\Delta x$ by differentiation of the function $\forall$ obtained in Step 3 [Eq. (2)]. This is approximated numerically as follows:

$$A(i\Delta x) = \frac{a_0}{gh_0}\frac{\forall\ [i\Delta t] - \forall\ [(i-1)\Delta t]}{\Delta t}, \quad i \in \{1, 2, \ldots, M\} \quad (6)$$

An example of the application of this step is shown in Appendix II.

Numerical Results and Discussion

To validate the proposed method, consider the case of a single pipe containing blockages of irregular shapes as shown in Fig. 2. Although it is difficult to choose blockage shapes that best mimic real blockages (because no information of this type appears to be collected in water supply pipe systems), the blockages considered in Fig. 2 are chosen for the purpose of illustration and for their generality.

The pipe section to be inspected is 2,000 m(=L) long, has a wave speed $a_0 = 1{,}000$ m/s, and is bounded by a valve on the left ($x = 0$) as shown in Fig. 1. The knowledge of the right boundary condition is not needed for the application of the proposed method. Any type of boundary is allowed after $x = L$. In other words, at $x > L$ there could be a pump, a dead end, a reservoir, or a network of pipes, or any other system that maintains a steady state. This is the reason that the boundary condition at $x = L$ is not shown in Fig. 1. The pressure head and the flow rate are considered to be initially ($t < 0$) constants, $H(x,t) = H_0 = 50$ m and $Q(x,t) = Q_0 = 0$.

The method of characteristics (MOC) (Wylie et al. 1993; Chaudhry 2014) is used to simulate the transient at every $\Delta x = 2.5$ m and $\Delta t = \Delta x/a = 2.5 \times 10^{-3}$ s. The area $A(x)$ is discretized accordingly. Data are collected for $t \in [0, 2L/a_0 = 4$ s]. At time $t = -\Delta t$, a transient is generated by a sudden opening and closing of the valve (i.e., during the time interval $[-\Delta t, +\Delta t]$).

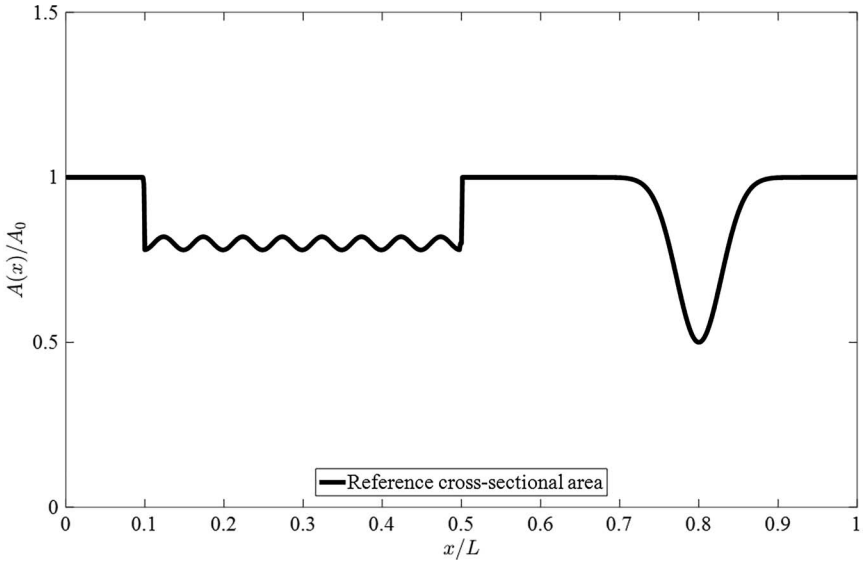

Fig. 2. Normalized pipe cross-sectional area $A(x)/A_0$ function of the normalized longitudinal coordinate x/L of the reference pipe (to be estimated).

J. Hydraul. Eng., 2019, 145(6): 04019019

The maximum flow rate after the valve opening is recorded at time $t = 0$ s and is equal to 1 m^3/s. The valve is fully closed when $t \geq \Delta t$. The pressure head is measured at the location $x = 0$ for a time $t \in [0.0\text{ s}, 4.0\text{ s}]$. The measured pressure head is not the impulse response function because the input is not a true unit impulse. To derive the impulse response function from the measured pressure head, the pressure head variation is normalized by $\int_{-\infty}^{\infty} Q(0,t)dt$. That is, $H(0,t) - H_0$ is divided by $\forall_0 = \int_{-\infty}^{\infty} Q(0,t)dt$, which is equal to 2.5×10^{-3} m^3 in this case. In practice, an impulse of flow can be approximated by a pulse that can be performed in different ways, such as a rapid injection of fluid (Brunone et al. 2008), a rapid opening or the closing of a valve (Lee et al. 2010). Furthermore, other transient generation methods, such as rapid closure of a downstream valve and pseudo-random binary signal, can be used to obtain an IRF (Lee 2005).

Following the steps of the algorithm outlined in the previous section and using the IRF obtained from numerical simulation (MOC), the internal pipe area is reconstructed and shown in Fig. 3. As shown, the reconstructed area using the proposed method and the reference area used in the forward problem coincide. This illustrates that the proposed method has the ability to accurately identify blockages of different sizes and shapes.

Comparison with Other Methods

To illustrate the advantages of the proposed method, it is compared with two other blockage detection methods using the same numerical test case as in Fig. 3. One method for comparison assumes a blocked pipe to be a series of pipes of different diameters as in [Fig. 1(b)] and is presented first. Then a second method for comparison using area reconstruction is presented. Both methods require knowledge of the right boundary conditions and the total length of the pipe. In this numerical simulation, the right boundary condition is considered to be a constant level reservoir located at $x = L_0 = 2{,}250$ m. This information is not needed in the proposed method. Moreover, as the two alternate methods use resonant frequencies, a $20 \times 4L_0/a_0$ numerical simulation time is considered to ensure high resolution in the frequency domain. Note that the advantage of the proposed method is that it only uses a measurement of $2L/a_0$ duration and does not require knowledge of the boundary condition at the right end of the pipe.

The sampling frequency used for the numerical simulation is maintained as in the previous test; that is, $f_s = 1/\Delta t = 400$ Hz. The 400-Hz frequency band considered contains about 1,800 resonant frequencies [the resonant frequencies for an intact pipe are given by $f_{rn} = (2n-1) \times a_0/4L_0$].

Resonant Frequencies Matching

The method described here is based on the regular blockage assumption [Fig. 1(b)] and is referred to as resonant frequencies matching (RFM). It is proposed in Duan et al. (2012b) and validated numerically and experimentally in Duan et al. (2013), Meniconi et al. (2013), and Duan (2016). The method uses eigenfrequency values to constrain the system dispersion relation using an optimization technique.

Only the first 30 resonant frequencies are used for the application of the RFM because use of all resonant frequencies (1,800) would incur a large computational cost. To apply RFM (Duan et al. 2012b), an a priori assumption must be made as to the number of blockages existing in the inspected pipe. When a single blockage is assumed, only three parameters need to be obtained (blockage location, blockage length and blockage size). Blockage detection results for a single blockage obtained by RFM are indicated by a continuous black line in Fig. 4.

It is clear that RFM with one blockage gives poor results, as it detects only one of the two blockages, identifying its midlength location but not its total length along the pipe.

Another possible assumption is that the pipe contains two blockages; that is, it is made up of five sections. In this case, the problem has eight unknown parameters (length and size of each pipe section). To reduce the unknowns of the problem (from eight to six), the area of the pipes beyond the blockages (Pipes 1, 3, and 5 counting from the valve location $x = 0$) is assumed equal the intact pipe area A_0. It should be noted that genetic algorithms give different results at different simulations. This is because the optimization function is highly nonconvex and contains several local minima Therefore, to increase the chance of convergence, the optimization process is repeated 50 times and the optimal solution with the least

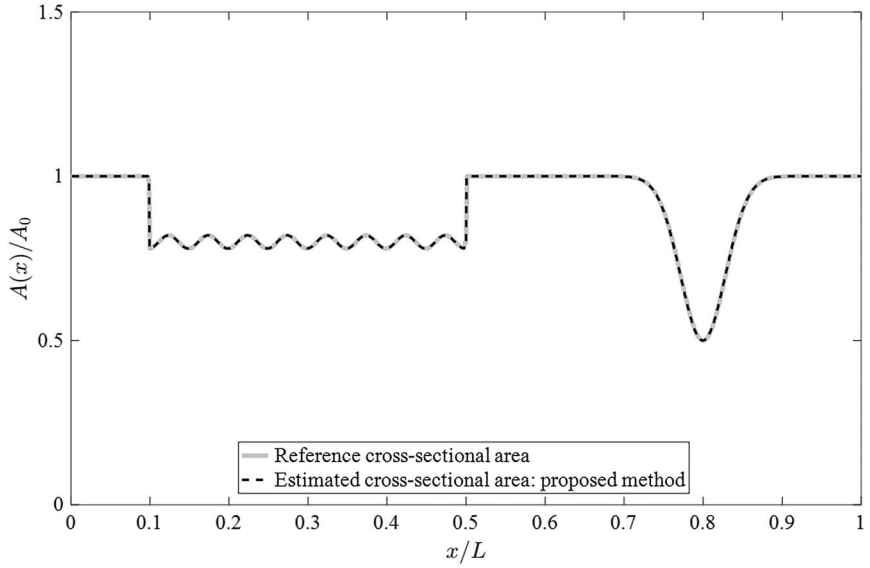

Fig. 3. Normalized pipe cross-sectional area function of the normalized longitudinal coordinate for two cases. Case 1 (gray): reference; and Case 2 (dashed black): estimated from proposed method.

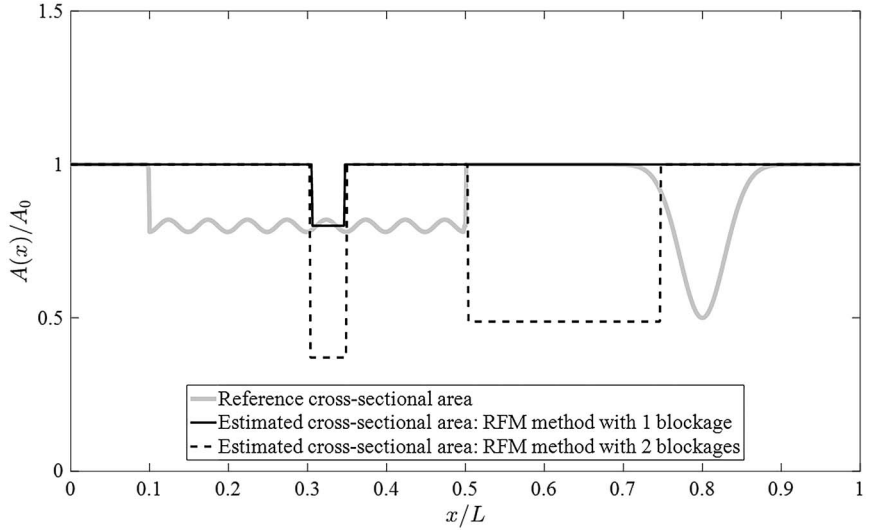

Fig. 4. Normalized pipe cross-sectional area function of the normalized longitudinal coordinate for three cases. Case 1 (gray): reference; Case 2 (solid black): estimated from RFM method assuming one blockage; and Case 3 (dashed black: estimated from RFM method assuming two blockages).

penalty is chosen. The result for this case is indicated by the dashed black line in Fig. 4. Again, the results of the RFM with two blockages are poor.

Of course, one may increase the number of assumed blockages to improve the results for this case where the internal pipe area is known. It would, however, be impossible to do this in practice since the number of blockage sections cannot be known a priori. Moreover, the more blockages one assumes, the less computationally efficient RFM becomes (Duan et al. 2012b). The same drawbacks apply to other regular blockage detection methods (e.g., Scola et al. 2017; Zouari et al. 2017).

Perturbation-Based Area Reconstruction

Perturbation-based area reconstruction (PAR) is an area reconstruction method that uses perturbation theory to derive an explicit relation between the pipe area and the measured resonant frequencies (Schroeder 1967; Heinz 1967). It is a simple and computationally efficient method for area reconstruction, which was used by Qunli and Fricke (1990) for blockage detection in the cooling systems of nuclear power plants. More recently, De Salis and Oldham (1999, 2001) proposed a similar method requiring fewer measurements.

PAR is easier than RFM in the sense that no assumptions need to be made regarding blockage shape or number and no optimization is involved. However, it requires an additional numerical simulation where the reservoir located at $x = 2{,}250$ m is replaced by a closed valve. The resonant frequencies for this case (valve-pipe-valve) are obtained in the same way as in the previous case (valve-pipe-reservoir). The two sets of resonant frequencies, one from valve-pipe-reservoir and another from valve-pipe-valve, are used to reconstruct the area using PAR as proposed by Qunli and Fricke (1990). In this case, all resonant frequencies in the band from 0 to 400 Hz are used. Results are shown in Fig. 5.

It can be seen in Fig. 5 that blockage locations and shapes are well predicted. However, PAR gives less accurate results compared with the proposed method (results shown in Fig. 3). In fact, two issues are observed. First, the area function is somehow shifted up. This is due to error in what is referred to by Qunli and Fricke (1990) as the "DC term," which is the constant term in the Fourier series of the area. This term cannot be determined from the eigenfrequency shift and can therefore only be approximated. The second issue is that, even if the shifting along the area axis is resolved, there remains an up and down variation between the two actual blockages that might mistakenly be construed as a third blockage. If the extended blockage (shown on the left in Fig. 5) is more severe, then the fictitious variation can be higher. Therefore, PAR is sensitive to blockage severity and/or sharp variations in the cross-sectional area.

In summary, the proposed method has the following advantages compared with the methods discussed previously:

- It gives more accurate results than the RFM and PAR methods.
- It uses only the impulse response function measured at a single location for a time $2L/a_0$ s (i.e., the part of the signal that is most reliable).
- It does not require a priori knowledge of all boundary conditions in the system and the total length of the pipe.
- Most important, it does not require a priori assumptions regarding blockage shape or number of blockages, and it applies to arbitrary blockage profiles.

Correction for Friction

In the previous section and in the derivation of the algorithm, the flow is assumed to be inviscid for simplicity. This section shows how friction effects are included in the proposed method.

Duan et al. (2012a) showed that the transient response in the case of viscous flow can be written as a frictionless response multiplied by a friction envelope

$$H^F(0,t) - H_0^F(0) \approx e^{-R|Q_0|t/2}[H(0,t) - H_0] \tag{7}$$

where $H_0^F(x)$ and H_0 = steady-state pressure head for cases with and without friction, respectively; Q_0 = steady-state flow rate; $H^F(x,t)$ and $H(x,t)$ = pressure head fluctuations for cases with and without friction, respectively. In this case, only the steady-state friction model is considered. That is, the wall shear is given by $\rho f Q|Q|/8A^2$, where f is the Darcy-Weisbach friction factor; ρ is the density; and A is the constant area of the pipe. Hence, R in Eq. (7) is given by $R = f\sqrt{\pi}/4A^{3/2}$. However, unsteady friction may be accounted for in a similar way (Duan et al. 2012a). Since the cases of primary interest in this paper are those for which area $A(x)$ is not constant, the envelope equation with a constant area should be thought of as an approximation for varying area.

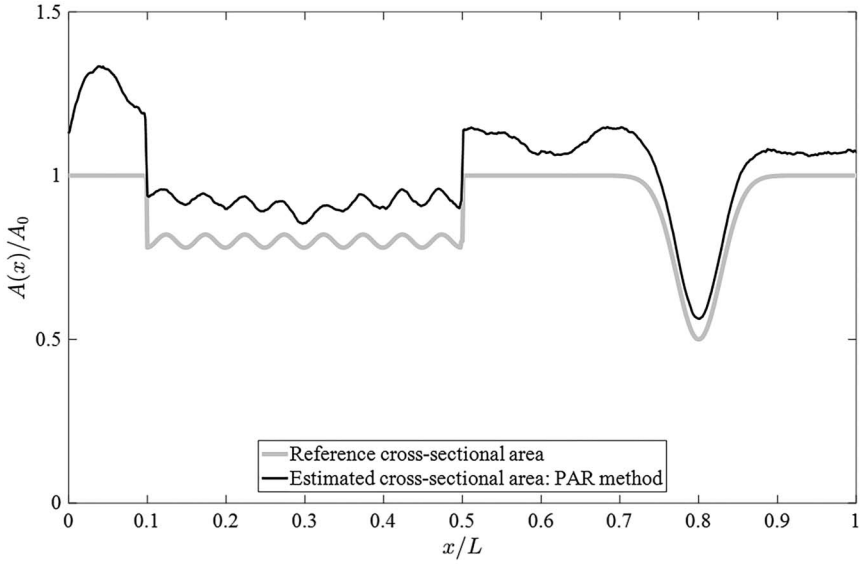

Fig. 5. Normalized pipe cross-sectional area function of the normalized longitudinal coordinate for two cases. Case 1 (bold grey): reference; and Case 2 (continuous black): estimated from PAR method.

To show the validity of the area reconstruction algorithm for friction and initial flow, the numerical example with the pipe cross-sectional area as in Fig. 2 is again considered. An initial steady-state flow rate is given as $Q(x, t < 0) = Q_0 = 1$ m^3/s, the friction factor is assumed to be $f = 0.02$, and the pressure head at the valve is $H(0, t < 0) = 46.96$ m. At time $t = 0$, the valve is suddenly closed; that is, at time $t = \Delta t$ the valve is completely closed. The method of characteristics (Chaudhry 2014) is used to obtain the pressure head response at the valve $H^F(0, t)$.

As far as the area reconstruction algorithm is concerned, the only change is in Step 1. The required change is to apply Eq. (7) to estimate the pressure head response for the frictionless case $H(0, t)$ from the measured pressure head response $H^F(0, t)$. Once the frictionless pressure head response $H(0, t)$ is obtained, the same algorithm steps (described in the previous section) can be used to estimate the internal cross-sectional area along the pipe.

Since the transient is generated by a rapid valve closure, further processing is performed to obtain the IRF, which will be used for the reconstruction. In this example, the IRF, $\Gamma(t)$, is obtained by $\Gamma(t) = (1/Q_0)/T_c[H(0, t + T_c) - H(0, t)]$, where T_c is the valve closure time.

Fig. 6 shows the exact area and the area reconstructed from the pressure head response under friction. It indicates that the area reconstruction is still accurate; that is, the blockages, location, size, and shape are accurately identified. It can be seen from the figure that the area after $x/L > 0.5$ is slightly smaller than the actual area. This is because the friction envelope assumes that area is constant along the pipe so large changes in area, as occur at the blockage centered at $x/L = 0.8$, induce more errors.

These numerical examples show that the area reconstruction method can be applied to general blockage types. The flow can be viscous or inviscid, and the transient can be generated in various

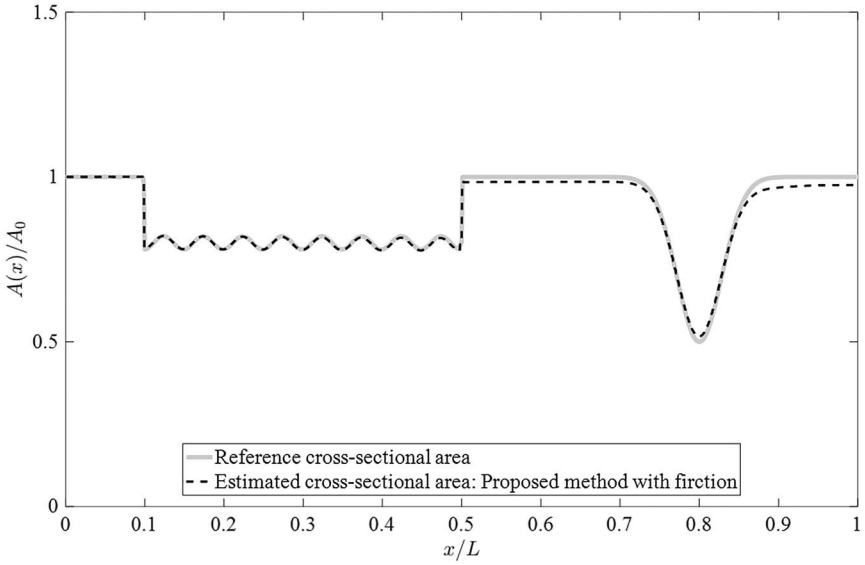

Fig. 6. Normalized pipe cross-sectional area function of the normalized longitudinal coordinate for two cases. Case 1 (gray): reference; and Case 2 (dashed black): estimated from proposed method when friction is considered.

ways provided that the IRF can be obtained. The blockage detection results for the numerical cases are highly accurate.

Conclusions

In this paper, an area reconstruction method was proposed as a tool for blockage detection. Fundamental physical and theoretical bases for the derivation of the method were discussed, and numerical tests, with and without friction, were considered to validate the method. The proposed method gives highly accurate results for general cases of multiple blockages of different shapes.

The proposed area reconstruction method was compared with other area reconstruction methods as well as with a regular blockage detection method. It was shown that the proposed method requires less information than other methods, in the sense that it needs only a single time measurement of duration $2L/a$ and does not require (a priori) knowledge of the system boundaries. Moreover, the proposed method makes no assumptions regarding the number of blockages or their shapes. This gives more accuracy in the results and makes the proposed method more practical for realistic applications.

The method is undergoing further validation with experimental data. Current work in progress shows that the proposed method can be extended to a branched network system (i.e., without loops).

Appendix I. Derivation of the Inverse Method

Problem Statement

Consider the linear water hammer equations on a finite segment $[0, L]$. Let g be the constant of gravity; $a(x)$, the wave speed at $x \in [0, L]$; and $A(x)$, the pipe cross-sectional area at x. If $H(x, t)$ and $Q(x, t)$ denote the change in the background pressure head and pipe discharge at x and time $t \geq 0$, the one-dimensional frictionless water hammer model is given by Wylie et al. (1993) and Ghidaoui et al. (2005) as

$$\frac{\partial H}{\partial t} + \frac{a^2(x)}{gA(x)}\frac{\partial Q}{\partial x} = 0 \tag{8}$$

$$\frac{\partial Q}{\partial t} + gA(x)\frac{\partial H}{\partial x} = 0 \tag{9}$$

with initial conditions on $x \in [0, L]$ of

$$H(x, 0) = 0, \qquad Q(x, 0) = 0 \tag{10}$$

These conditions mean that the pipe is unperturbed at time $t = 0$. Note that $H(x, t)$ is used here to denote perturbation in the pressure head, whereas in the main text $H(x, t)$ is the overall pressure head.

Two boundary conditions are imposed: (1) a control valve at $x = 0$ and (2) an arbitrary condition $x = L$. In this case, the transient is generated by changing the flow $Q(0, t)$ and the pressure head $H(0, t)$ is measured for $t \geq 0$. The purpose is to find information about $a(x)$ and $A(x)$ inside the pipe $x \in [0, x_{\max}]$ from the measured pressure head $H(0, t)$.

Comments about the Algorithm

The proposed algorithm was originally suggested by Sondhi and Gopinath (1971) for reconstructing the shape of vocal tracts. It recovers the area $A(x)$ for a vocal tract of known constant wave speed. In this paper, the method is further extended to recover either the wave speed [if $A(x)$ is known] or the cross-sectional area [if $a(x)$ is known] in a segment $[0, x_{\max}]$. This is done by measuring the pressure $H(0, t)$ for time t in a finite time interval after generating a transient flow by an impulse of flow $Q(0, t) = \forall_0 \delta(t)$, where $\forall_0$ is the volume injected by the impulse. The following paragraphs discuss various concepts needed for the algorithm and then a step-by-step solution method.

Impulse Response

If the flow is governed by the water hammer Eqs. (8)–(10), an impulse boundary source $Q(0, t) = \forall_0 \delta(t)$ is applied at $x = 0$ and an unknown boundary condition is applied at $x = L$, the impulse response function is then defined to be the normalized measured pressure variation and is denoted $\Gamma(t)$. Linearity of the model guarantees that these data are enough to reconstruct the response to any kind of input flow $Q(0, t)$ by convolution. Hence, for a general input $Q(0, t)$ the pressure head measurement $H(0, t)$ is given by

$$H(0, t) = (Q * \Gamma)(t) = \int_{-\infty}^{\infty} Q(0, s)\Gamma(t - s)ds \tag{11}$$

Note that $\Gamma(t) = 0$ for $t < 0$ because the pipe is unperturbed then. Similarly, $Q(0, s) = 0$ whenever $s < 0$. Thus, the integral is actually $H(0, t) = \int_0^t Q(0, s)\Gamma(t - s)ds$.

Travel Time Coordinates

If $t \geq 0$, the travel time coordinate $x(t)$ is defined as the point x that a perturbation from $x = 0$ would reach in time t. It is given by the unique solution $x(t)$ to either

$$t = \int_0^{x(t)} \frac{dx}{a(x)} \quad \text{or} \quad x(t) = \int_0^t a[x(\tau)]d\tau \tag{12}$$

In the case of constant wave speed $x(t) = a_0 t$.

Boundary Integral Identity

In this section, an integral identity that gives information on the region $x > 0$ from time domain measurements at the boundary $x = 0$ is calculated. Let H and Q satisfy the model Eqs. (8)–(10). Fix $\tau > 0$ such that $x(\tau) < L$ and integrate Eq. (8) on $[0, L] \times [0, \tau]$. Then

$$-\int_0^\tau \int_0^L \frac{\partial Q}{\partial x}(x, t)dxdt = \int_0^\tau \int_0^L \frac{gA(x)}{a^2(x)}\frac{\partial H}{\partial t}(x, t)dxdt \tag{13}$$

Note, however, that $Q(x, t) = H(x, t) = 0$ when $x > x(t)$ because of the finite speed of propagation. After switching the order of integration on the right and noting that $H(x, t) = Q(x, t) = 0$ when $x > x(\tau)$, the last equation becomes

$$\int_0^\tau Q(0, t)dt = \int_0^{x(\tau)} \frac{gA(x)}{a^2(x)}H(x, \tau)dx \tag{14}$$

Constant Pressure

Given $\tau > 0$ the strategy in this algorithm is to choose a boundary source $Q(0, t) = Q_{1,\tau}(0, t)$ such that at $t = \tau$ the corresponding pressure $H(x, t) = H_{1,\tau}(x, t)$ is constant h_0 in $[0, x(\tau)]$ and zero elsewhere. The question is how to build such a function. Note that the constant functions $\mathcal{H}(x, t) = 2h_0$ and $\mathcal{Q}(x, t) = 0$ satisfy Eqs. (8) and (9). The theory of Cauchy problems for hyperbolic partial differential equations (e.g., Garabedian 1964) implies the

following: if the boundary data satisfy $\mathcal{H}(0,t) = 2h_0$ and $\mathcal{Q}(0,t) = 0$ for time $0 < t < 2\tau$, then $\mathcal{H}(x,t) = 2h_0$ and $\mathcal{Q}(x,t) = 0$ in the triangular region $x < x(\tau - |\tau - t|)$.

Let $H_{1,\tau}(x,t)$ and $Q_{1,\tau}(x,t)$ satisfy Eqs. (8) and (9). Then so do $\mathcal{H}$ and $\mathcal{Q}$ defined by

$$\mathcal{H}(x,t) = H_{1,\tau}(x,t) + H_{1,\tau}(x,2\tau - t) \tag{15}$$

$$\mathcal{Q}(x,t) = Q_{1,\tau}(x,t) - Q_{1,\tau}(x,2\tau - t) \tag{16}$$

Imposing the boundary conditions $\mathcal{H}(0,t) = 2h_0$ and $\mathcal{Q}(0,t) = 0$ for $0 < t < 2\tau$ makes, by the previous paragraph, $\mathcal{H} = 2h_0$ and $\mathcal{Q} = 0$ in the triangular region $x < x(\tau - |\tau - t|)$. Both conditions $\mathcal{H} = 2h_0$ and $\mathcal{Q} = 0$ are required; otherwise, $\mathcal{H} = 2h_0$ and $\mathcal{Q} = 0$ are not guaranteed in the triangular region $x < x(\tau - |\tau - t|)$. These conditions are used in the next section to deduce a boundary equation. At $t = \tau$, Eq. (15) gives

$$2h_0 = \mathcal{H}(x,\tau) = H_{1,\tau}(x,\tau) + H_{1,\tau}(x,\tau) \tag{17}$$

therefore $H_{1,\tau}(x,\tau) = h_0$ for all $0 < x < x(\tau)$.

For any $\tau > 0$, then, the goal is to compute $H = H_{1,\tau}$ and $Q = Q_{1,\tau}$, satisfying Eqs. (8) and (9) and the initial conditions of Eq. (10), such that the functions $\mathcal{H}$ and $\mathcal{Q}$ from Eqs. (15) and (16) satisfy the boundary conditions $\mathcal{H}(0,t) = 2h_0$, $\mathcal{Q}(0,t) = 0$ for $0 < t < 2\tau$.

Boundary Integral Equation

The purpose of this subsection is to write, for a given time $\tau > 0$, an equation whose solution is the input $Q_{1,\tau}(0,t)$, which produces the constant pressure change $H_{1,\tau}(x,\tau) = h_0$ for $x < x(\tau)$. As discussed in the previous subsection, this can be achieved by choosing $\mathcal{Q}(0,t) = 0$ and $\mathcal{H}(0,t) = 2h_0$ for $0 < t < 2\tau$. This implies that $Q_{1,\tau}(0,t) = Q_{1,\tau}(0,2\tau - t)$ and $H_{1,\tau}(0,t) + H_{1,\tau}(0,2\tau - t) = 2h_0$ in that same time interval. Using Eq. (11) gives

$$\int_{-\infty}^{\infty} Q_{1,\tau}(0,s)\Gamma(t-s)ds + \int_{-\infty}^{\infty} Q_{1,\tau}(0,s)\Gamma(2\tau - t - s)ds = 2h_0 \tag{18}$$

In the second integral change the variable s to $s' = 2\tau - s$; note that $Q_{1,\tau}(0,s) = Q_{1,\tau}(0,2\tau - s)$ as seen above. Then

$$\int_{-\infty}^{\infty} Q_{1,\tau}(0,s)\Gamma(t-s)ds + \int_{-\infty}^{\infty} Q_{1,\tau}(0,s')\Gamma(s'-t)ds' = 2h_0 \tag{19}$$

This gives an integral equation for $Q_{1,\tau}(0,t)$.

Integral Equation For Smooth Model

If the wave speed $a(x)$ and pipe cross-sectional area $A(x)$ are twice continuously differentiable functions, then the impulse response function has the following form:

$$\Gamma(t) = \frac{a(0)}{gA(0)}[\delta(t) + r_m(t)] \tag{20}$$

where $r_m(t)$ = continuously differentiable function (Sondhi and Gopinath 1971). Inserting this into Eq. (19) gives

$$2Q_{1,\tau}(0,t) + \int_{-\infty}^{\infty} Q_{1,\tau}(0,s)r_m(t-s)ds + \int_{-\infty}^{\infty} Q_{1,\tau}(0,s)r_m(s-t)ds = \frac{2gA(0)}{a(0)}h_0 \tag{21}$$

Recalling that $Q_{1,\tau}(0,s) = 0$ when $s < 0$, and since $Q_{1,\tau}(0,s) = Q_{1,\tau}(0,2\tau - s)$, then $Q_{1,\tau}(0,s) = 0$ for $s > 2\tau$. Moreover, $r_m(s-t) = 0$ when $s < t$, so the last equation becomes

$$2Q_{1,\tau}(0,t) + \int_{0}^{t} Q_{1,\tau}(0,s)r_m(t-s)ds + \int_{t}^{2\tau} Q_{1,\tau}(0,s)r_m(s-t)ds = \frac{2gA(0)}{a(0)}h_0 \tag{22}$$

or

$$Q_{1,\tau}(0,t) + \frac{1}{2}\int_{0}^{2\tau} Q_{1,\tau}(0,s)r_m(|t-s|)ds = \frac{gA(0)}{a(0)}h_0 \tag{23}$$

which is a Fredholm integral equation of the second kind.

Solving for Cross-Sectional Area or Wave Speed

Assume now that, for any $0 < \tau < T$, the input pipe discharge function $Q(0,t) = Q_{1,\tau}(0,t)$, which would make the pressure head change $H(x,\tau)$ constant h_0 for position $0 < x < x(\tau)$, is known. The purpose of this subsection is to deduce $a(x)$ or $A(x)$ from $Q_{1,\tau}(0,t)$.

Define

$$\forall(\tau) = \int_{0}^{\tau} Q_{1,\tau}(0,t)dt \tag{24}$$

Recall that, by Eq. (14)

$$\forall(\tau) = \int_{0}^{x(\tau)} \frac{gA(x)}{a^2(x)}h_0 dx \tag{25}$$

for $0 < \tau < T$ [assume that $x(T) < L$]. Also recall that the definition of travel-time coordinates is

$$x(\tau) = \int_{0}^{\tau} a[x(s)]ds \tag{26}$$

By the chain rule

$$\forall'(\tau) = \frac{gA[x(\tau)]}{a^2[x(\tau)]}h_0 x'(\tau) = \frac{gA[x(\tau)]}{a^2[x(\tau)]}h_0 a[x(\tau)] = \frac{gA[x(\tau)]}{a[x(\tau)]}h_0 \tag{27}$$

where $\forall'$ = derivative of V with respect to τ. Eq. (27) shows that local hydraulic impedance is recovered at a different travel-time distance $x(\tau)$.

There are a few options for recovering $a(x)$ or $A(x)$ at any given point x as follows:

- If $a(x)$ is constant a_0, then

$$A(x) = \frac{\forall'(x/a_0)a_0}{gh_0} \tag{28}$$

- If $A(x)$ is a constant A_0, then the situation is slightly more complicated. The travel time coordinate $x(t)$ is first obtained at $t = t_0$

$$x(t_0) = \int_{0}^{t_0} a[x(\tau)]d\tau = \int_{0}^{t_0} \frac{gA_0}{\forall'(\tau)}h_0 d\tau \tag{29}$$

J. Hydraul. Eng., 2019, 145(6): 04019019

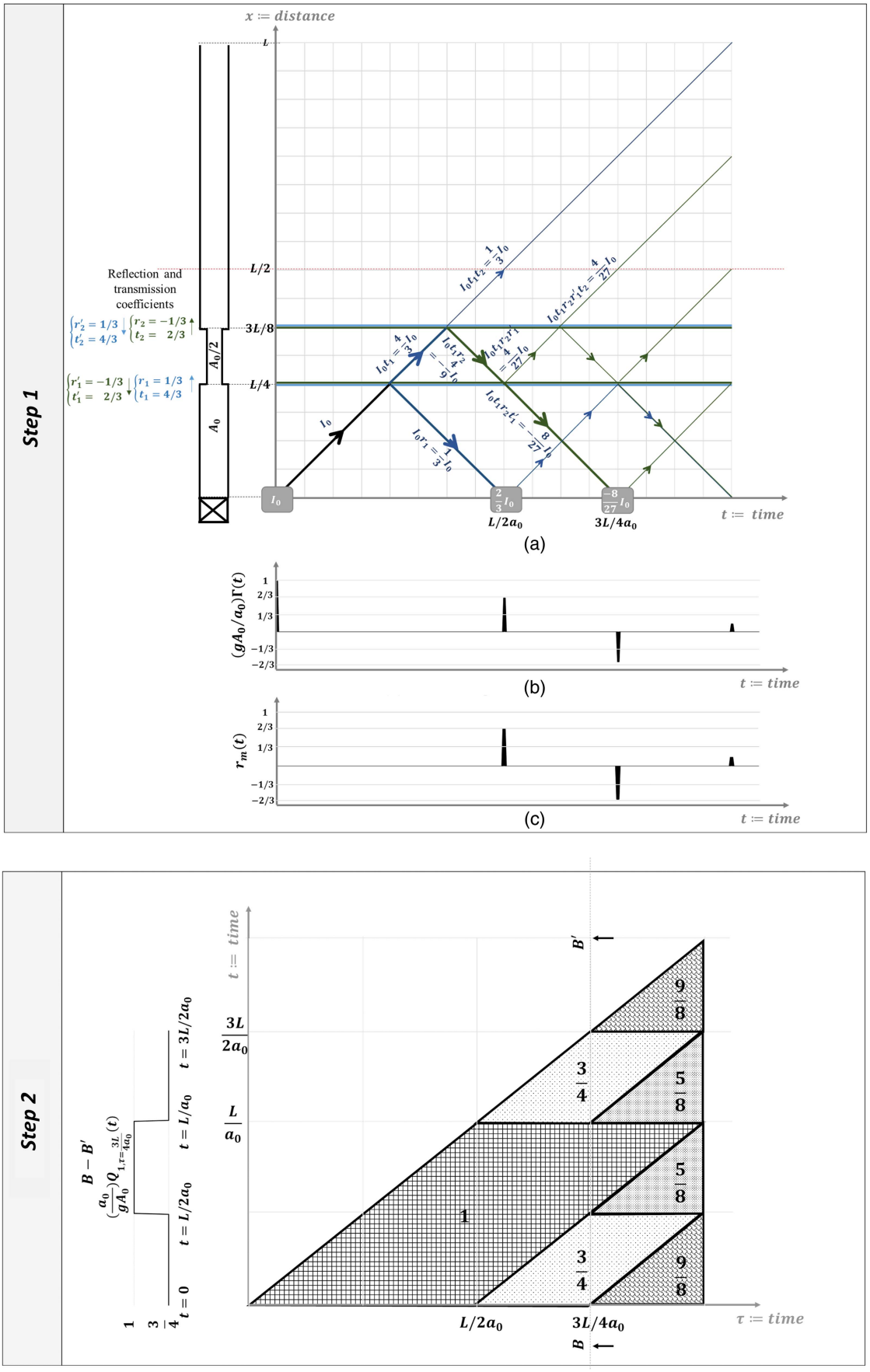

Fig. 7. Algorithm steps through an example: (a) space-time wave propagation; (b) impulse response function; (c) reflected impulse response; (d) computed input $Q_{1,\tau}(t)$; (e) integral of $Q_{1,\tau}(t)$; and (f) reconstructed area $A(x)$.

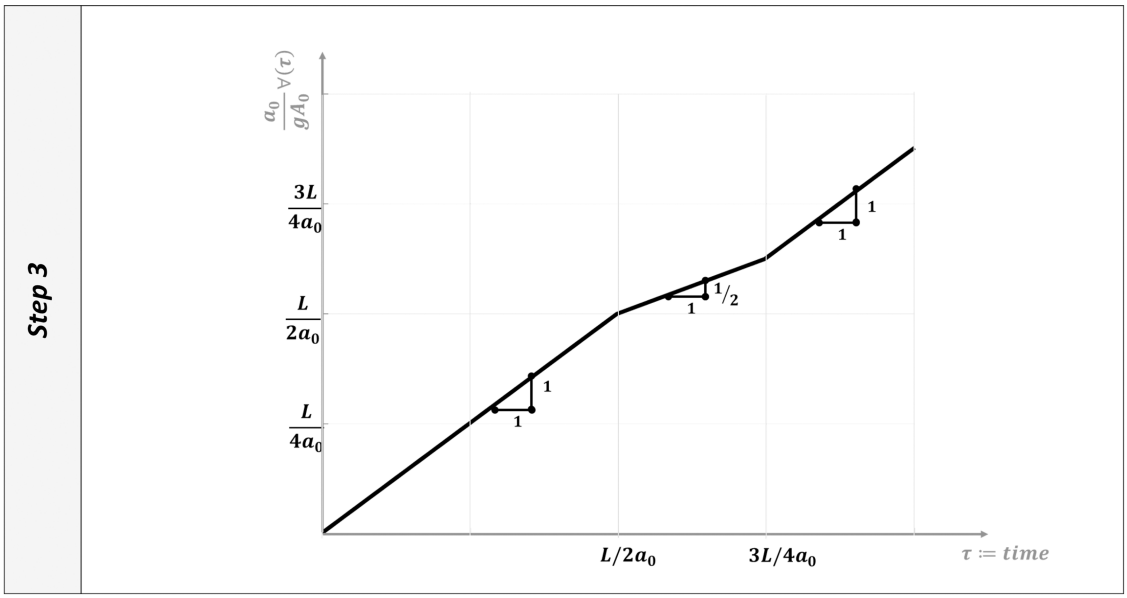

(e)

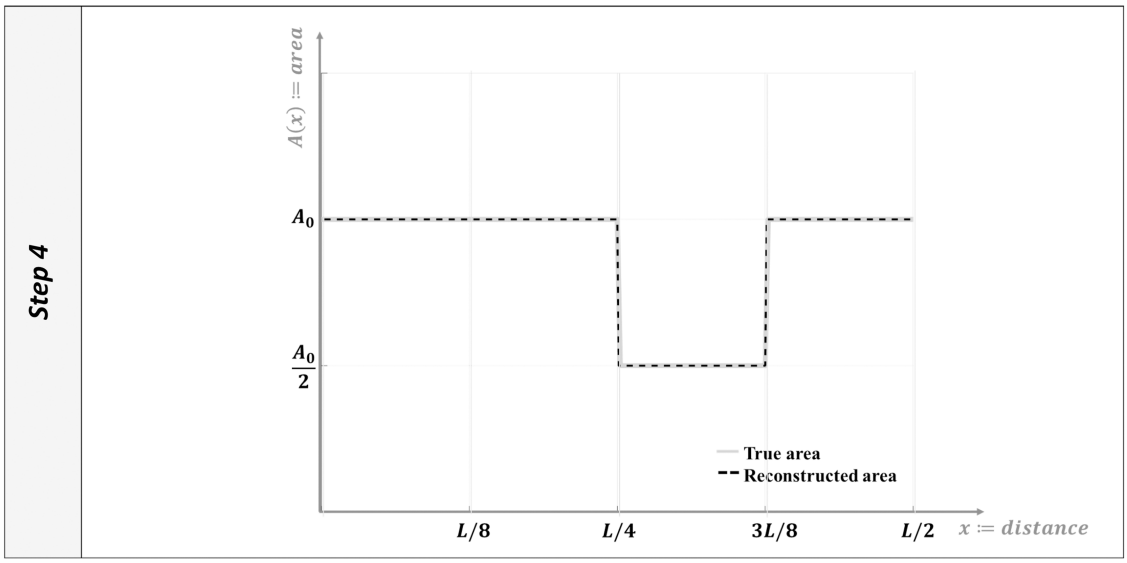

(f)

Fig. 7. (*Continued.*)

Then the wave speed $a(x)$ at $x = x(t_0)$ is obtained by

$$a(x) = a[x(t_0)] = \frac{gA_0}{\forall'(t_0)}h_0 \tag{30}$$

- If $a(x)$ or $A(x)$ are known but not constants, first $x(t)$ is obtained in the same way as above and then $A(x)$ or $a(x)$, respectively, is obtained through Eq. (27).
- If neither $a(x)$ nor $A(x)$ are known, but there is a known relation between a and A, the wave speed $a[x(\tau)]$ can be solved from Eq. (27) and then $x(\tau)$ from Eq. (26) and a fortiori $a(x)$ and $A(x)$ as in the second option in this list.

Appendix II. Algorithm Steps through an Example

Consider a simple pipe of length L in which the wave speed is a constant equal to a_0. The internal pipe area is A_0 everywhere except in the region from $x = L/4$ to $x = 3L/8$, in which region the area is equal to $A_0/2$. A sketch of the pipe is shown vertically for convenience in Fig. 7(a).

The reflection and transmission coefficients for a wave traveling from the valve at $x = L/4$ are $r_1 = 1/3$ and $t_1 = 4/3$ and at $x = 3L/8$ are $r_2 = -1/3$ and $t_2 = 2/3$. The reflection and transmission coefficients for a wave traveling toward the valve are $r_{1'} = -1/3$ and $t_{1'} = 2/3$ at $x = L/4$ and $r_{2'} = 1/3$ and $t_{2'} = 4/3$ at $x = 3L/8$. The wave propagation in the pipe is illustrated in an $x - t$ diagram in Fig. 7(a). The vertical axis is the x-axis, which coincides with the longitudinal axis of the pipe. The horizontal axis is the time axis, which is discretized as $\Delta t = \Delta x/a_0$, where Δx is the discretization step in space. The scattering of a wave generated at the valve ($x = 0$, $t = 0$) is traced in the $x - t$ diagram and is only shown up to $t = L/a_0$. The area $A(x)$ is reconstructed up to $x = L/2$ for ease of discussion. The magnitude of the reflected and transmitted waves are computed from the reflection and transmission coefficients and are shown in Fig. 7(a). It is noted that the

magnitude of a wave reflected at the valve is doubled because waves are fully reflected at a closed valve (or dead end).

The pressure head response to a unit impulse of flow generated at the valve (IRF) is shown in Fig. 7(b). The signal $r_m(t)$ is therefore extracted from the measured pressure head as discussed in Step 1 of the proposed algorithm and is shown in Fig. 7(c).

The measured signal $r_m(t)$ in the interval $[0, 2\tau]$ is used to compute the special input $Q_{1,\tau}(t)$ for $t \in [0, 2\tau]$. This gives a large set of curves $Q_{1,\tau}(t)$, which are shown in Fig. 7(d). The horizontal axis represents the time τ, the vertical axis is the time t and the different patterns indicates different values of $Q_{1,\tau}(t)$. For example, at $\tau = 3L/4a_0$, $(a_0/gA_0)Q_{1,\tau}(t)$ is equal to 3/4 when $t \in [0, L/2a_0] \cup]L/a_0, 3L/2a_0]$ and equal to 1 when $t \in]L/2a_0, L/a_0]$. $Q_{1,\tau=3L/4a_0}(t)$ is shown at the left in Fig. 7(d) as a cut B-B' of the right plot at the right in Fig. 7(d).

In Step 3, the integral with time t of $Q_{1,\tau}(t)$ is computed at different τ and its corresponding values $\forall(\tau)$ are shown in Fig. 7(e). In Step 4, the area $A(x)$ is easily computed by differentiating $\forall(\tau)$ with τ. The area $A(x)$ is shown in Fig. 7(f) together with the reference area.

Appendix III. Numerical Solution of the Integral Equation in the Main Text

When Eq. (1) is written for different discrete time values $t = \{0, \Delta t, 2\Delta t \ldots, (2N-1)\Delta t\}$ with $N\Delta t = \tau$, it becomes a system of equations

$$
\begin{aligned}
&Q_{1,\tau}(0,0) + \frac{1}{2}\int_0^{2\tau} Q_{1,\tau}(0,s) r_m(|s|) ds = \frac{gA(0)}{a(0)} h_0 \\
&Q_{1,\tau}(0,\Delta t) + \frac{1}{2}\int_0^{2\tau} Q_{1,\tau}(0,s) r_m(|\Delta t - s|) ds = \frac{gA(0)}{a(0)} h_0 \\
&\vdots \\
&Q_{1,\tau}[0,(2N-1)\Delta t] \\
&\quad + \frac{1}{2}\int_0^{2\tau} Q_{1,\tau}(0,s) r_m(|(2N-1)\Delta t - s|) ds = \frac{gA(0)}{a(0)} h_0
\end{aligned} \tag{31}
$$

If $r_m(t)$ is also discretized with the same discrete time domain $\mathbf{r}_m = \{r_m(0), r_m(\Delta t), \ldots, r_m[(2N-1)\Delta t]\}$, then the integral $\int_0^{2\tau} Q_{1,\tau}(0,s) r_m(|t-s|) ds$ can be approximated by a rectangular approximation as follows:

$$
\int_0^{2\tau} Q_{1,\tau}(0,s) r_m(|t-s|) ds = \sum_{j=0}^{2N-1} Q_{1,\tau}(0, i\Delta t) r_m(|t - i\Delta t|) \Delta t \tag{32}
$$

Hence, the previous system of equations becomes

$$
\begin{aligned}
&Q_{1,\tau}(0,0) + \frac{1}{2}\sum_{j=0}^{2N-1} Q_{1,\tau}(0, j\Delta t) r_m(j\Delta t)\Delta t = \frac{gA(0)}{a(0)} h_0 \\
&Q_{1,\tau}(0,\Delta t) + \frac{1}{2}\sum_{j=0}^{2N-1} Q_{1,\tau}(0, j\Delta t) r_m(|\Delta t - j\Delta t|)\Delta t = \frac{gA(0)}{a(0)} h_0 \\
&\vdots \\
&Q_{1,\tau}[0,(2N-1)\Delta t] \\
&\quad + \frac{1}{2}\sum_{j=0}^{2N-1} Q_{1,\tau}(0, j\Delta t) r_m[|(2N-1)\Delta t - j\Delta t|]\Delta t = \frac{gA(0)}{a(0)} h_0
\end{aligned} \tag{33}
$$

Therefore, it can be written as

$$
\mathbf{H}\mathbf{q}_{1,\tau} = \frac{gA(0)}{a_0}\mathbf{h}_0 \tag{34}
$$

where $\mathbf{H} = 2N \times 2N$ matrix such that $\mathbf{H}(i,j) = \delta_{i,j} + \Delta t \times r_m(|i-j|\Delta t)/2$, in which $\delta_{i,j}$ = Kronecker delta function; $\mathbf{q}_{1,\tau}$ = a $2N \times 1$ vector with the ith element equal to $Q_{1,\tau}(0, 2i\Delta t)$, and $\mathbf{h}_0$ = a $2N \times 1$ vector with all elements equal to h_0.

Acknowledgments

This research is funded by the postgraduate studentship and by the Research Grant Council of the Hong Kong SAR, China [Project No. T21-602/15R, Smart Urban Water Supply Systems (Smart UWSS) and project No. 16203417]. The authors thank Prof. D. A. McInnis for the editorial suggestions.

Notation

The following symbols are used in this paper:

$A(x)$ = cross-sectional area of pipe at location x;
$a(x)$ = wave speed at location x in pipe;
a_0 = constant wave speed along pipe;
f = Darcy-Weisbach friction factor;
g = constant acceleration due to gravity;
$H(x,t)$ = pressure head at location x and time t for frictionless pipe;
$H^F(x,t)$ = pressure head at location x and time t when friction is considered;
H_0 = steady-state pressure head for frictionless pipe;
$H_0^F(x)$ = steady-state pressure head at location x when friction is considered;
$\mathbf{H}$ = matrix obtained from $r_m(t)$ and used for numerical calculations;
h_0 = added constant pressure head created by injecting input $Q_{1,\tau}$;
$\mathbf{h}_0$ = vector with all elements equal to h_0;
L = length of pipe section to be inspected;
L_0 = total length of pipe;
N = variable integer number such as $N\Delta t = \tau$;
$Q(x,t)$ = flow rate at location x and time t;
Q_0 = steady-state flow rate;
$Q_{1,\tau}(t)$ = artificial input flow rate which creates constant pressure h_0 along pipe at time τ;
$\mathbf{q}_{1,\tau}$ = vector obtained from $Q_{1,\tau}(t)$ and used for numerical calculations;
R = term defined for convenience that depends on friction factor and pipe area;
$r_m(t)$ = normalized reflected impulse response (RIR);
s = time variable;
T = time constant that satisfies $x(T) < L$;
t, t_0 = time variables;
x = axial coordinate;
$\delta(t)$ = Dirac delta function, or unit impulse;
$\Gamma(t)$ = impulse response function;
$\mathcal{H}$ = pressure head that satisfies condition $\mathcal{H}(x,\tau) = 2h_0$;
$\mathcal{Q}$ = flow rate that satisfies condition $\mathcal{Q}(x,\tau) = 0$;
ρ = density of fluid in pipe;

τ = time at which pressure head becomes constant;
$\forall_0$ = volume of fluid injected during impulse injection; and
$\forall(\tau)$ = volume of fluid injected in time interval $[0, \tau]$.

References

Belishev, M. I. 1997. "Boundary control in reconstruction of manifolds and metrics (the BC method)." *Inverse Prob.* 13 (5): R1. https://doi.org/10.1088/0266-5611/13/5/002.

Bonder, L. J. 1983. "Equivalency of lossless n-tubes." *Acta Acustica United Acustica* 53 (4): 193–200.

Bruckstein, A. M., and T. Kailath. 1987. "Inverse scattering for discrete transmission-line models." *SIAM Rev.* 29 (3): 359–389. https://doi.org/10.1137/1029075.

Brunone, B., M. Ferrante, and S. Meniconi. 2008. "Portable pressure wavemaker for leak detection and pipe system characterization." *J. Am. Water Work Assoc.* 100 (4): 108–116. https://doi.org/10.1002/j.1551-8833.2008.tb09607.x.

Chaudhry, M. H. 2014. *Applied hydraulic transients*. 3rd ed. New York: Springer.

Chen, C. T. 1998. *Linear system theory and design*. 3rd ed. New York: Oxford University Press.

De Salis, M., and D. Oldham. 1999. "Letters to the editor." *J. Sound Vib.* 221 (1): 180–186. https://doi.org/10.1006/jsvi.1998.1965.

De Salis, M., and D. Oldham. 2001. "The development of a rapid single spectrum method for determining the blockage characteristics of a finite length duct." *J. Sound Vib.* 243 (4): 625–640. https://doi.org/10.1006/jsvi.2000.3433.

Duan, H. 2016. "Sensitivity analysis of a transient-based frequency domain method for extended blockage detection in water pipeline systems." *J. Water Resour. Plann. Manage.* 142 (4): 04015073. https://doi.org/10.1061/(ASCE)WR.1943-5452.0000625.

Duan, H., M. S. Ghidaoui, P. J. Lee, and Y. K. Tung. 2012a. "Relevance of unsteady friction to pipe size and length in pipe fluid transients." *J. Hydr. Eng.* 138 (2): 154–166. https://doi.org/10.1061/(ASCE)HY.1943-7900.0000497.

Duan, H. F., P. J. Lee, M. S. Ghidaoui, and Y. K. Tung. 2012b. "Extended blockage detection in pipelines by using the system frequency response analysis." *J. Water Resour. Plann. Manage.* 138 (1): 55–62. https://doi.org/10.1061/(ASCE)WR.1943-5452.0000145.

Duan, H. F., P. J. Lee, A. Kashima, J. Lu, M. S. Ghidaoui, and Y. K. Tung. 2013. "Extended blockage detection in pipes using the system frequency response: Analytical analysis and experimental verification." *J. Hydr. Eng.* 139 (7): 763–771. https://doi.org/10.1061/(ASCE)HY.1943-7900.0000736.

Eisner, E. 1967. "Complete solutions of the 'Webster' horn equation." *J. Acoust. Soc. Am.* 41 (4B): 1126–1146. https://doi.org/10.1121/1.1910444.

El-Raheb, M., and P. Wagner. 1982. "Acoustic propagation in rigid ducts with blockage." *J. Acoust. Soc. Am.* 72 (3): 1046–1055. https://doi.org/10.1121/1.388236.

Garabedian, P. R. 1964. *Partial differential equations*. New York: Wiley.

Ghidaoui, M. S., M. Zhao, D. A. McInnis, and D. H. Axworthy. 2005. "A review of water hammer theory and practice." *Appl. Mech. Rev* 58 (1): 49–76. https://doi.org/10.1115/1.1828050.

Gong, J., M. F. Lambert, A. R. Simpson, and A. C. Zecchin. 2014. "Detection of localized deterioration distributed along single pipelines by reconstructive MOC analysis." *J. Hydr. Eng.* 140 (2): 190–198. https://doi.org/10.1061/(ASCE)HY.1943-7900.0000806.

Gopinath, B., and M. M. Sondhi. 1970. "Determination of the shape of the human vocal tract from acoustical measurements." *Bell Syst. Tech. J.* 49 (6): 1195–1214. https://doi.org/10.1002/j.1538-7305.1970.tb01820.x.

Heinz, J. M. 1967. "Perturbation functions for the determination of vocal-tract area functions from vocal-tract eigenvalues." *STL-QPSR* 8 (1): 001–014.

Lee, P. J. 2005. "Using system response functions of liquid pipelines for leak and blockage detection." Ph.D. thesis, Dept. of Civil and Environmental Engineering, Univ. of Adelaide.

Lee, P. J., J. P. Vítkovský, M. F. Lambert, A. R. Simpson, and J. Liggett. 2010. "Leak location in pipelines using the impulse response function." *J. Hydr. Res.* 45 (5): 643–652. https://doi.org/10.1080/00221686.2007.9521800.

Louati, M., S. Meniconi, M. S. Ghidaoui, and B. Brunone. 2017. "Experimental study of the eigenfrequency shift mechanism in a blocked pipe system." *J. Hydr. Eng.* 143 (10): 04017044. https://doi.org/10.1061/(ASCE)HY.1943-7900.0001347.

Massari, C., T. C. J. Yeh, M. Ferrante, B. Brunone, and S. Meniconi. 2015. "A stochastic approach for extended partial blockage detection in viscoelastic pipelines: Numerical and laboratory experiments." *J. Water Supply Res. Technol. Aqua* 64 (5): 583–595. https://doi.org/10.2166/aqua.2015.034.

Meniconi, S., H. F. Duan, P. J. Lee, B. Brunone, M. S. Ghidaoui, and M. Ferrante. 2013. "Experimental investigation of coupled frequency and time-domain transient test-based techniques for partial blockage detection in pipelines." *J. Hydr. Eng.* 139 (10): 1033–1040. https://doi.org/10.1061/(ASCE)HY.1943-7900.0000768.

Mohapatra, P. K., M. H. Chaudhry, A. A. Kassem, and J. Moloo. 2006. "Detection of partial blockage in single pipelines." *J. Hydrol. Eng.* 132 (2): 200–206. https://doi.org/10.1061/(ASCE)0733-9429(2006)132:2(200).

Qunli, W., and F. Fricke. 1990. "Determination of blocking locations and cross-sectional area in a duct by eigenfrequency shifts." *J. Acoust. Soc. Am.* 87 (1): 67–75. https://doi.org/10.1121/1.398914.

Sattar, A. M., M. H. Chaudhry, and A. A. Kassem. 2008. "Partial blockage detection in pipelines by frequency response method." *J. Hydrol. Eng.* 134 (1): 76–89. https://doi.org/10.1061/(ASCE)0733-9429(2008)134:1(76).

Schroeder, M. R. 1967. "Determination of the geometry of the human vocal tract by acoustic measurements." *J. Acoust. Soc. Am.* 41 (4B): 1002–1010. https://doi.org/10.1121/1.1910429.

Scola, I. R., G. Besançon, and D. Georges. 2017. "Blockage and leak detection and location in pipelines using frequency response optimization." *J. Hydr. Eng.* 143 (1): 04016074. https://doi.org/10.1061/(ASCE)HY.1943-7900.0001222.

Sondhi, M. 1979. "Estimation of vocal-tract areas: The need for acoustical measurements." *IEEE Trans. Acoust. Speech Sig. Process.* 27 (3): 268–273. https://doi.org/10.1109/TASSP.1979.1163240.

Sondhi, M., and J. R. Resnick. 1983. "The inverse problem for the vocal tract: Numerical methods, acoustical experiments, and speech synthesis." *Acoust. Soc. Am. J.* 73 (3): 985–1002. https://doi.org/10.1121/1.389024.

Sondhi, M. M., and B. Gopinath. 1971. "Determination of vocal tract shape from impulse response at the lips." *J. Acoust. Soc. Am.* 49 (6B): 1867–1873. https://doi.org/10.1121/1.1912593.

Wang, X. J., M. F. Lambert, and A. R. Simpson. 2005. "Detection and location of a partial blockage in a pipeline using damping of fluid transients." *J. Water Resour. Plann. Manage.* 131 (3): 244–249. https://doi.org/10.1061/(ASCE)0733-9496(2005)131:3(244).

Wylie, E. B., V. L. Streeter, and L. Suo. 1993. *Fluid transients in systems*. 6 ed. Upper Saddle River, NJ: Prentice-Hall.

Zouari, F., X. Wang, M. Louati, and M. S. Ghidaoui. 2017. "Single extended blockage identification using a model-based matched-field processing approach." In *Proc., 36 IAHR World Congress*. Beijing: International Association of Hydraulic Research.